IVYSPRING INTERNATIONAL PUBLISHER

Nanotheranostics

2017; 1(2): 186 -195. doi: 10.7150/ntno.18619

Research Paper

Gadolinium and Platinum in Tandem: Real-time Multi-Modal Monitoring of Drug Delivery by MRI and Fluorescence Imaging

Hongguang Li[1], Bethany I. Harriss[2], Alkystis Phinikaridou[3], Sara Lacerda[3], Gregory Ramniceanu[5, 6], Bich-Thuy Doan[5, 6], Ka-Lok Ho[1], Chi-Fai Chan[1, 4], Wai-Sum Lo[4], René M. Botnar[3], Rongfeng Lan[1], Cyrille Richard[5, 6]✉, Ga-Lai Law[4]✉, Nicholas J. Long[2]✉ and Ka-Leung Wong[1]✉

1. Department of Chemistry, Hong Kong Baptist University, Kowloon Tong, Kowloon, Hong Kong SAR;
2. Department of Chemistry, Imperial College London, South Kensington Campus, London SW7 2AZ, UK;
3. King's College London, Division of Imaging Sciences, Lambeth Wing, St Thomas' Hospital London SE1 7EH;
4. Department of Applied Biology and Chemical Technology, Hong Kong Polytechnic University, Hung Hom, Hong Kong SAR;
5. Unité de Technologies Chimiques et Biologiques pour la Santé (UTCBS); CNRS UMR 8258; Inserm U 1022; Université Paris Descartes, Sorbonne Paris Cité, Faculté des Sciences Pharmaceutiques et Biologiques, 75006 Paris, France;
6. Chimie-ParisTech, PSL, 75005 Paris, France.

✉ Corresponding authors: Ka-Leung Wong, PhD., Department of Chemistry, Hong Kong Baptist University, Kowloon Tong, Kowloon, Hong Kong SAR. Tel: 852-3411-2370. E-mail: klwong@hkbu.edu.hk; or Nicholas J. Long, PhD., Department of Chemistry, Imperial College London, South Kensington Campus, London SW7 2AZ, UK. Fax: +44 20 7594 5804; Tel: +44 20 7594 5781; E-mail: n.long@imperial.ac.uk or Ga-Lai Law, PhD., Department of Applied Biology and Chemical Technology, Hong Kong Polytechnic University, Hung Hom, Hong Kong SAR. E-mail: ga-lai.law@polyu.edu.hk or Cyrille Richard, PhD., Unité de Technologies Chimiques et Biologiques pour la Santé (UTCBS); CNRS UMR 8258; Inserm U 1022; Université Paris Descartes, Sorbonne Paris Cité, Faculté des Sciences Pharmaceutiques et Biologiques, 75006 Paris, France and Chimie-ParisTech, PSL, 75005 Paris, France. E-mail: cyrille.richard@parisdescartes.fr.

Received: 2016.12.06; Accepted: 2017.04.11; Published: 2017.05.08

Abstract

A novel dual-imaging cisplatin-carrying molecular cargo capable of performing simultaneous optical and MR imaging is reported herein. This long-lasting MRI contrast agent (r_1 relaxivity of 23.4 $mM^{-1}s^{-1}$ at 3T, 25 °C) is a photo-activated cisplatin prodrug (**PtGdL**) which enables real-time monitoring of anti-cancer efficacy. **PtGdL** is a model for monitoring the drug delivery and anti-cancer efficacy by MRI with a much longer retention time (24 hours) in several organs such as renal cortex and spleen than GdDOTA and its motif control **GdL**. Upon complete release of cisplatin, all **PtGdL** is converted to **GdL** enabling subsequent MRI analyses of therapy efficacy within its reasonably short clearance time of 4 hours. There is also responsive fluorescence enhancement for monitoring by photon-excitation.

Key words: prodrug; multi-modal; MRI; drug delivery; fluorescence imaging; cisplatin.

Introduction

Highly cytotoxic platinum (II)/(IV) coordination complexes, such as cisplatin and its derivatives, i.e. carboplatin/oxaliplatin, are well-known potent anticancer agents (1-5). Their pharmacologically inactive forms, otherwise termed as prodrugs, have been developed for optimizing their drug delivery process, e.g. tumor selectivity, water solubility, and cell permeability, before subsequent activation at the target sites (6-8). Despite the clinical success of several prodrugs, unprecedented challenges remain in achieving their desired pharmacokinetics with minimal adverse side effects since they are non-specifically distributed throughout the body (9). The major drawback of prodrugs, according to the literature, lies in the difficulties of tracing their activities *in vitro/in vivo* (10-11). Intriguingly, the recent advent of theranostic nanomedicine – an emerging paradigm combining diagnostic and therapeutic entities into one – creates a new research landscape and provides a promising solution to the prodrug conundrum (12-14).

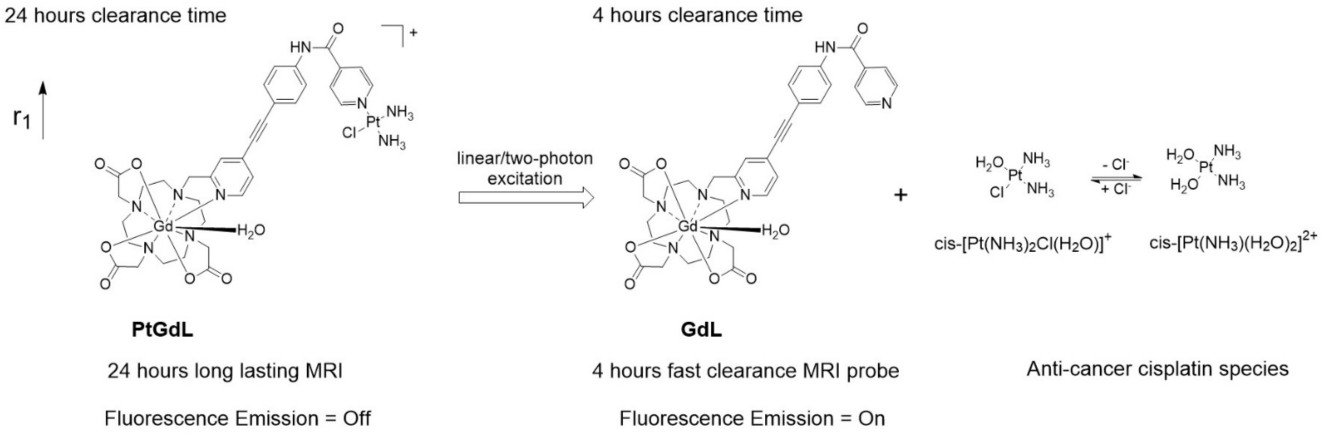

Figure 1. Schematic illustration of the photo-induced cleavage of the multi-modal long-lasting MRI contrast agent (**PtGdL**) to generate a fast clearance MRI probe (**GdL**) simultaneously showing highly fluorescent off–on signals and cytotoxic effects.

Novel theranostic technology affords simultaneous imaging diagnosis and targeted therapy for diseases (15-17). For instance, theranostic nanoagents of diagnostic capability and therapeutic efficacy can be utilized in pathological mechanistic studies and guided pre-/post-treatment assessments due to their responsive signaling, e.g. magnetic resonance (MR) and fluorescence *in vitro/in vivo* (18-20). The biodistribution characteristics of a theranostic scaffold *in vivo* are necessary to be recorded to assess the efficiency of drug or probe delivery to pathological tissues. Such agents would allow us to control the drug release with the fluorescence excitation and monitor the drug's therapeutic effect with the emission of the prodrug (21-22). Borrowing the concept from their nano-counterparts, our goal is to develop theranostic molecular prodrugs. Recently, we reported a proof-of-concept study on our newly designed platinum-europium complex (**PtEuL**) which holds great promise as a controlled delivery vehicle of cisplatin. It shows real-time, responsive photo-triggered 'off-on' lanthanide-based long-lived fingerprint emission during the drug delivery to therapeutic process *in vitro* once cisplatin is photo-dissociated (23). However, deep penetration *in vivo* imaging, such as in internal organs, with the previous methodology is impossible. Our present goal of developing a dual-imaging cisplatin-carrying molecular cargo capable of performing simultaneous optical and MR imaging, i.e. synergistic sensitive and high temporal-spatial resolution, will help scientists to study the real-time biodistribution and pharmacokinetics *in situ* more comprehensively and conveniently. In addition, this complex will assist the evaluation of the performance of the prodrug without interference from autofluorescence, not to mention the advantage of avoiding tedious control experiments (24-26).

Herein, we have achieved the breakthrough of an 'all-in-one' fluorescence imaging, MRI and photo-dissociable theranostic agent **PtGdL** (Figure 1) with much larger r_1 relaxivity (23.4 $mM^{-1}s^{-1}$, 3T, 25°C) and longer retention (24 hours) MR imaging compared to GdDOTA and **GdL** (controls). The longer retention time in renal cortex (i.e. between 4-18 hours) provides the duration for the cisplatin from **PtGdL** to be released, enabling anti-cancer therapy (conditions) via photon irradiation. Following this, **PtGdL** is converted to the fast clearance motif form, **GdL**, allowing further therapy analysis and is cleared over a short period of time.

Results and Discussion

Photophysical and photochemical properties of the prodrug PtGdL

The solution-state electronic adsorption and emission spectra of **GdL** and **PtGdL** were determined at 298 K in aqueous solution. The **GdL** complex is the proposed product of **PtGdL** after photo-irradiation and was used to monitor the photo-induced delivery of $[Pt–(NH_3)_2Cl]^+$ from **PtGdL**. The absorption bands of **PtGdL** and **GdL** are located at *ca.* 327 and 324 nm respectively (Figure 2A). **GdL** exhibited relatively strong blue emission peaking at around 426 nm, with 3 % quantum yield, in aqueous solution, which is attributed to the ligand fluorescence. **PtGdL** is non-emissive since the excited states (singlet excited state S_1 or triplet excited state T_1) of the ligand chromophore are quenched by the cisplatin moiety. The energy transfer and quenching mechanism of the platinum moiety to the organic chromophore of **PtGdL** is similar compared with our previous study of **PtEuL** (23). In **PtGdL**, the energy absorbed by the organic chromophore is transferred to the dissociative state (23) of the cisplatin moiety in **PtGdL,** which weakens the Py–Pt coordination bond, and subsequently results in the dissociation of the cisplatin moiety instead of generating fluorescence. The difference in photophysical property of **GdL** and **PtGdL** offers a responsive emission signal change upon UV or two-photon excitation of the **PtGdL** complex, resulting in the delivery of cisplatin moiety and **GdL** from the complex **PtGdL**. Photo-activation of **PtGdL** in tris buffer solution is shown in Figure 2C. The pseudo-first order rate constant k for the dissociation of the cisplatin unit in **PtGdL** is 0.051 min^{-1}, which is similar to our reported motif complex **PtEuL** (ks **=** 0.053 min^{-1}, under same conditions as **PtGdL**) (23). The emission intensity of the organic antenna of **PtGdL** was enhanced 48-fold after the photo-release of the cisplatin unit from **PtGdL**.

In vitro two-photon imaging and *in vitro*/*in vivo* photodynamic therapeutic effects of PtGdL

The dark toxicity of the **PtGdL** complex was evaluated in a cancer cell line (HeLa) and a normal cell line (WPMY-1) (Table S3 and Figure S3). **PtGdL** showed lower dark toxicity compared to pure cisplatin over 24 hours (IC_{50} of cisplatin in HeLa = ~3.3 ± 0.3 µM and WPMY-1 = 4.2 ± 0.6 µM; **PtGdL** in HeLa = ~23.6 ± 0.8 µM and WPMY-1 = 43.9 ± 1.1 µM). The UVA (365 nm, $1Jcm^{-2}$) induced photo-cytotoxicity of **PtGdL** is about seven times higher than its dark toxicity (light IC_{50} of **PtGdL** in HeLa = ~3.8 ± 0.7 µM and WPMY-1 = ~6.9 ± 1.1 µM) and it is comparable with the dark cytotoxicity of cisplatin in HeLa and WPMY-1 cells. In the control experiments, cisplatin and **GdL** show similar photo cytotoxicity to their dark cytotoxicity. However UV light suffers from disadvantages such as short penetration depth and DNA damage of UV light itself. The photo-cytotoxicity of **PtGdL** was further investigated on a Leica SP8 (upright configuration) confocal microscope equipped with an NIR femtosecond laser. Real-time photo-release of cisplatin from **PtGdL** in HeLa can be monitored and image by the photo-induced responsive emission during the photoactivation of **PtGdL**. For photo-cytotoxicity, the two-photon *in vitro* imaging and photo-release of cisplatin in human cervical cancer cells (HeLa) were investigated on a Leica SP8 (upright configuration) confocal microscope equipped with a femtosecond laser. The blue-green emission from the cells treated with **PtGdL** was observed in the cytoplasm with significant toxicity at the excitation of 730 nm laser for 30 min (420 mW power within 30 min, 5 min duration, steady temperature = 37 °C ± 1.5 °C). Dramatic cell death can be observed with less than 5 µM dosage concentration with **PtGdL**, however, the dark IC_{50} of **PtGdL** against HeLa cells is ~23.6 µM under the same experimental conditions (Figure 3 and Figure S3). Control experiments were performed with **GdL** under the same experimental conditions and no significant cell death was observed from either **GdL** treatment or laser irradiation.

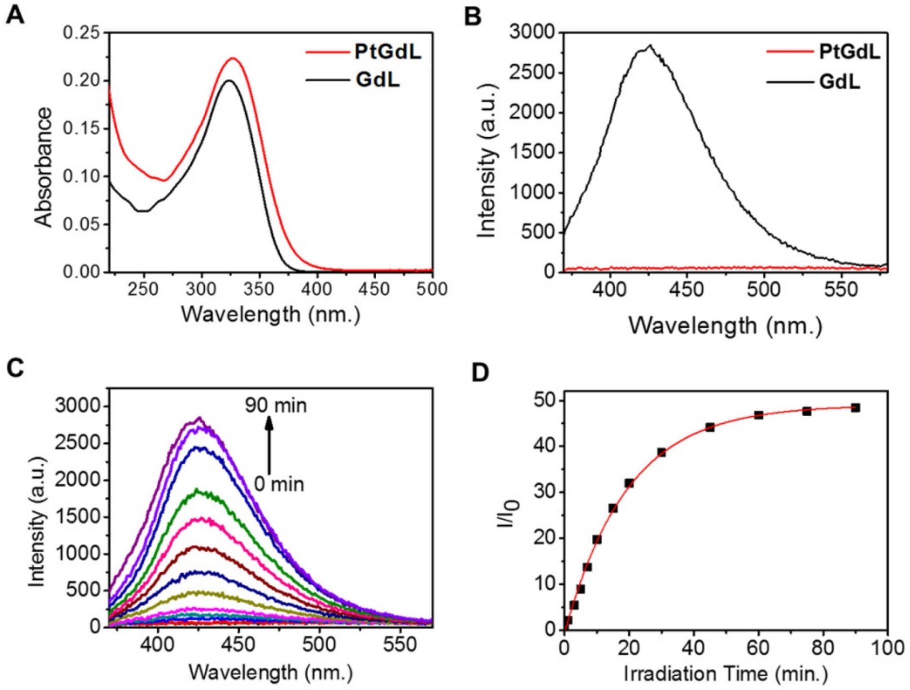

Figure 2. Photophysical and photochemical properties of **PtGdL** and **GdL** in tris buffer solution: Absorption (A, 10 µM) and emission spectra (B, 3 µM, λ_{ex} = 330 nm) of **PtGdL** and **GdL**; Emission spectra variation of 3 µM of **PtGdL** (C) in tris buffer solution (20 mM tris base, 50 mM NaCl, pH 7.4) with irradiation of 365 nm UV light. (D) Plot of I/I_0 @ 426 nm vs. time. Pseudo-first order rate constant for the dissociation of **PtGdL** is 0.051 min^{-1}.

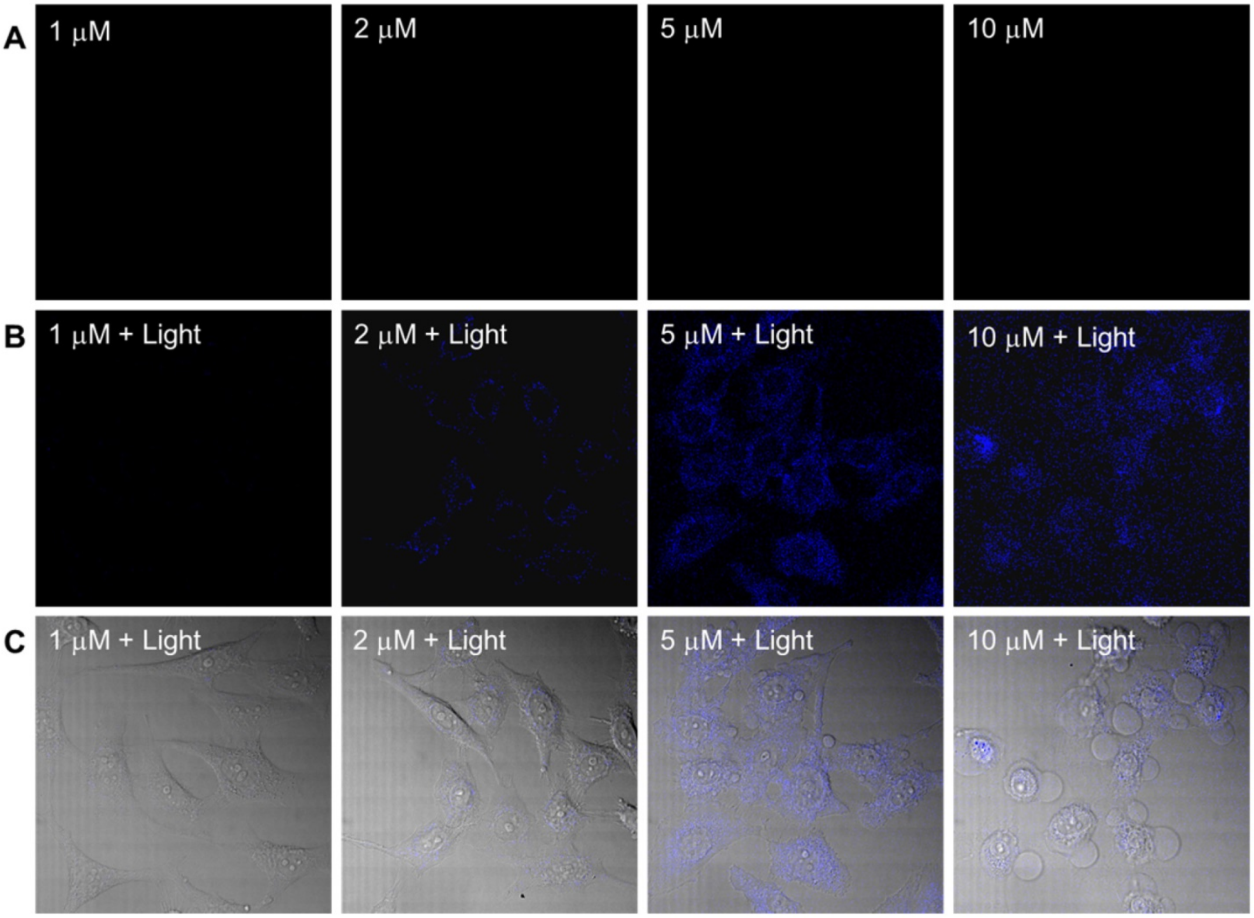

Figure 3. Two-photon (λ_{ex} = 730 nm) induced images and cell death of HeLa cells incubated with **PtGdL** at different dose concentrations (1, 2, 5, 10 μM) for 24 h. (A) Without irradiation, there is no blue emission; (B) after 30 min excitation, blue emission from released **GdL** was observed; (C) Merged images of (B) and bright field of (A) shows significant cell death and blue emission intensity from the cells treated with **PtGdL** and 730 nm laser (Remark : IC_{50} of **PtGdL** in HeLa cells is 23.6 ± 0.8 μM).

To evaluate the *in vivo* photodynamic anticancer ability of **PtGdL,** intra-tumoral injections of PBS buffer, cisplatin (2.5 mg per kg) and **PtGdL (**9.6 mg per kg) were administered to HeLa cell xenografts in BALB/c nude mice. The injections were carried out once every two days in the dark. The tumor treated with **PtGdL** was irradiated with 365 nm UVA (10 mW) for 30 min after 30 min of the injection. After irradiation of UVA, the mice were returned to dark. The treatments continued for 14 days. At the end of the experiment, the mice were killed and the tumors were excised and weighed. **PtGdL** with UVA irradiation showed comparable tumor growth inhibition compared to the tumor injected with PBS buffer (the size and the mass of the tumor are reduced to about one-third comparing with the tumor injected with PBS buffer). The experiments demonstrated that our prodrug **PtGdL** with UVA irradiation has similar anticancer effects with cisplatin. (Figure S4)

The T_1 relaxivity of PtGdL

One of the key breakthroughs of this work features the magnetic properties of **PtGdL**. The r_1 relativity of the proposed MR-available prodrug - **PtGdL** - has been measured and surprisingly, the relaxivity at 3T was six times greater than Gd-DOTA (Figure 4). The efficacy of **PtGdL** as a potential MRI contrast agent was evaluated by proton nuclear magnetic relaxation dispersion (NMRD). The proton NMRD profiles of the relaxivity – defined as the enhancement of longitudinal relaxation rate by 1 mM of a Gd(III) complex – of **PtGdL**, **GdL** and Gd-DOTA are shown in Figure 4. The profiles were run at 25 and 37°C, and the concentrations of the samples were confirmed by ICP-MS. Moreover, a high preliminary r_1 relaxivity of **PtGdL** of 23.4 $mM^{-1}s^{-1}$ was also measured at 3T (25°C), demonstrating its potential to be used as a T_1- weighted MRI contrast agent. The T_1 relaxation time of a set of 5 solutions of **PtGdL** of different concentrations was measured in a 3T Philips Achieva scanner. The concentration of the solutions was confirmed by ICP-MS and the relaxivity was determined by the plot of the relaxation rate (R_1, s^{-1}) as the function of the Gd(III) concentration in mM

(Figure S5, Table S4). The observed relaxivities for both **GdL** and **PtGdL** are unexpectedly high. We believe that these increased relaxivities are due to an aggregation of the compounds in solution, which results from the isonicotinamide group, leading to a stacking effect of the molecules. This effect becomes even more remarkable in the presence of the cisplatin unit – leading to an additional increase in the relaxivity of **PtGdL** when compared to **GdL**: 29.4 vs 23.1 $mM^{-1}s^{-1}$ at 10 MHz (0.25T) and 25 °C. The DLS measurement of an aqueous solution of **PtGdL** showed the presence of aggregates e.g. 672 ± 24 nm (single peak, PDI 0.156; Figure S6), which suggests that the increasing effect comes from high rotational correlation times due to the presence of aggregates in solution (27-30). The related compounds Gd-DO$_3$A-(4-morpholinopyridine) and the Gd-DTPA-(cisplatin-pyridine-2-ylmethanamine), reported in the literature, show a relaxivity of 5.3 $mM^{-1}s^{-1}$ (20 MHz and 25°C) and 6.5 $mM^{-1}s^{-1}$ (20 MHz, 37°C) respectively (31-32). The coordination sphere of the Gd(III) in our novel compounds and in the literature analogs is the same, featuring one water molecule (Table S2). The presence of the cisplatin unit directly conjugated to the pyridine only leads to a small increase of the relaxivity when compared to Gd-DOTA. These facts help support our conclusion that the increased relaxivities of our compounds result from the additional isonicotinamide group.

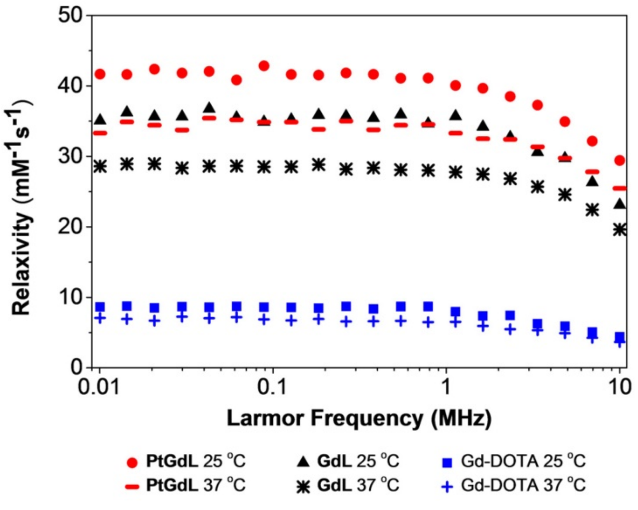

Figure 4. NMRD profiles of **PtGdL**, **GdL** and Gd-DOTA (1 mM) at different magnetic field strength values, and at 25 °C and 37°C.

MRI studies of PtGdL *in vivo*

Based on these interesting results, *in vivo* 7T MRI measurements were performed on normal wild-type mice to evaluate biodistribution of the imaging probes in different organs and to assess the pharmacokinetics. MR images were acquired at various time-points in different organs of interest (kidney, liver, and spleen) to record the kinetic uptake, retention and clearance of contrast agents of injected solutions of the commercially available Gd-DOTA complex (DOTAREM), **GdL** and **PtGdL**. The injection doses were, respectively, 210 μmol/kg (4 μmol/mouse) and 30 μmol/kg (0.6 μmol/mouse). After intravascular injection via the caudal vein, the uptake phase was visualized from the MR signal enhancement observed in the liver and renal cortex. **GdL** was immediately captured by the liver, spleen and the kidneys in 10s (Figure 5A and 6A). No specific retention was observed in any of the observed tissues. Full clearance was observed approximately 4 hours post-injection (Figure 5C and 6C). By the clearance phase, the signal enhancement of **GdL** had decreased by 90 %, indicating full clearance (Figure 5C). In comparison to commercialized Gd-DOTA, **GdL** presented a similar biodistribution pattern in the kidneys but a slower clearance rate in the liver (slope of signal intensity enhancement in the clearance part (0.002 vs 0.016 /min). However, **PtGdL**, showed a slightly delayed capture, longer retention, and slower clearance compared to **GdL**. The uptake delay increased from 6 to 9 minutes in the kidney and 9 to 15 min in the liver (Figures 5B and 6B) indicating prolonged retention in the bloodstream of the **PtGdL** relative to the other probes. This result is interesting as imaging or theranostic probes should be retained as long as possible because they generally have to reach their targets via the blood pathway. Hepatic and renal retention of about 24 hours was observed for **PtGdL**. The MRI signal enhancement decreased by 90% at 24 hours, indicating a clearance of the order of one day (Figure 5C). This long-lasting clearance may be due to an interaction between the cisplatin moiety in **PtGdL** and some proteins (33-37). The liver showed discoloration (whitening) compared to the normal reddish tissue color (data not shown here). In summary, **PtGdL** presents advantages compared to cisplatin-free **GdL**. In particular, **PtGdL** has the potential to become a new generation of MRI-available agents. The controlled photo-triggered release of cisplatin from **PtGdL** can serve as an anti-cancer drug delivery vehicle while the efficacy of the anti-cancer effects can be simultaneously monitored based on the untransformed **PtGdL**. Upon complete cleavage of cisplatin, i.e. complete generation of **GdL** from **PtGdL**, the remaining **GdL** is cleared within 4 hours, and the fate of cisplatin is well-studied in literature.

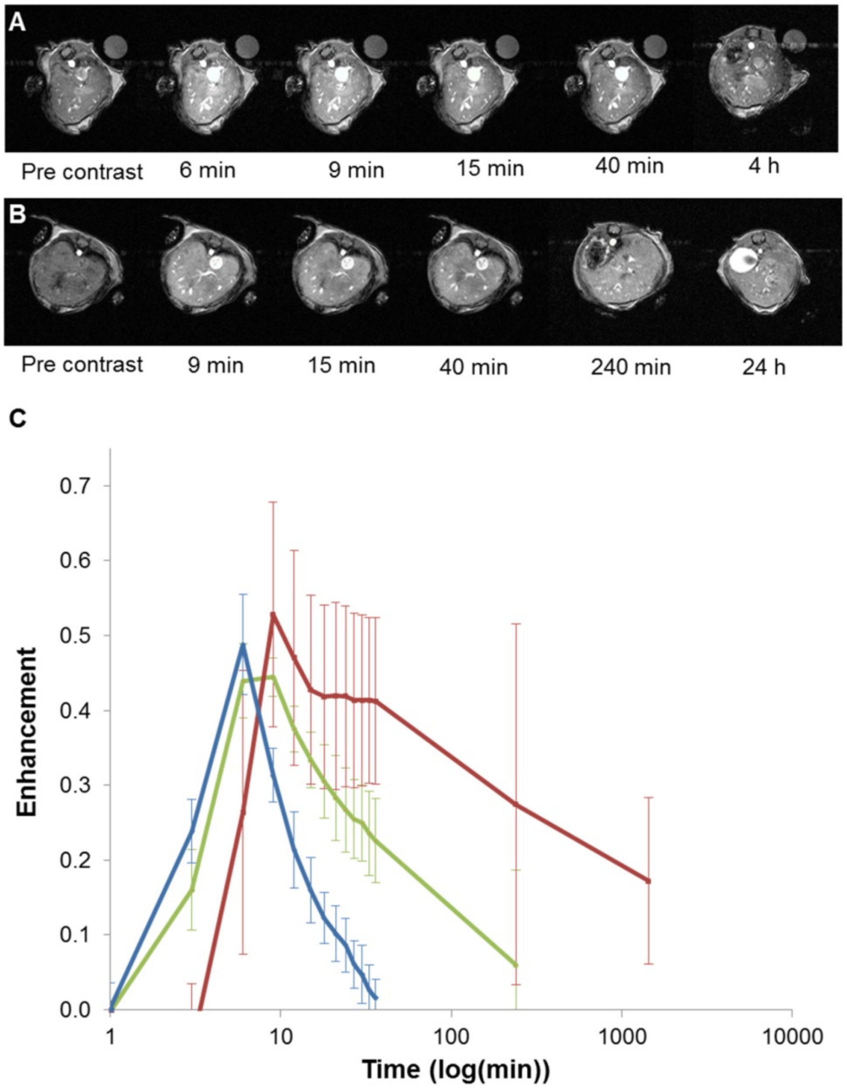

Figure 5. *In vivo* T_1-weighted MR images of mouse liver obtained between 6 minutes and 4 hours post injection for GdL (A) and between 9 minutes and 24 hours post injection for PtGdL (B). The signal-decay curves (red line: PtGdL, green line: GdL, blue line: Gd-DOTA) are represented in C.

Conclusions

In conclusion, we have advanced our previous photo-activated theranostic anti-cancer prodrug by incorporating excellent MRI capabilities (r_1 23.4 $mM^{-1}s^{-1}$ at 3T, 25 °C) as a tool for monitoring the arrival of the prodrug with low cytotoxicity. We can photo-assist release of cisplatin for therapy, with the cis-platin released from non-toxic **PtGdL** being observed by the emission of **GdL** (removal of cisplatin). In addition, **PtGdL** also exhibits longer retention time (24 hours) in target organ(s) than the cisplatin-free **GdL** and GdDOTA controls, thus allowing a wider timeframe for the released cisplatin to perform anti-cancer function and for monitoring. Upon completing release of cisplatin, all **PtGdL** is converted to **GdL** for subsequent responsive MR and fluorescence imaging analysis of therapy efficacy and biodistribution within its reasonably short clearance time of 4 hours. Our next step will focus on integrating these multifunctional prodrugs with target-specific vectors to enhance their specificity towards clinical targets and increasing the overall efficiency of the anti-cancer therapy.

Experimental Section

Synthesis and characterization of the complexes GdL and PtGdL

The synthesis and characterized in our previously work (23). The high performance liquid chromatography (HPLC) spectra and the high resolution ESI mass spectra of **GdL** and **PtGdL** are shown in the supporting information Figure S1 and S2.

Photophysical measurements

UV-Visible absorption spectra in the spectral range 200 to 1100 nm were recorded by an HP Agilent UV-8453 spectrophotometer. Emission spectra were recorded by using a Horiba Fluorolog-3 spectrophotometer. (Available for fluorescence lifetime and steady state emission measurement - equipped with a visible to near-infrared-sensitive photomultiplier in nitrogen flow cooled housing). The spectra were corrected for detector response and stray background light phosphorescence. The absolute emission quantum yields of **GdL** and **PtGdL** were measured by integrated sphere techniques (38). The linear light induced dissociation of **PtGdL** in tris buffer (20 mM tris base, 50 mM NaCl, pH 7.4) was monitored by determination of the emission spectra of solution of **PtGdL** in tris buffer with different light dosage of 365 nm UV light. 3 mL of the solution of **PtGdL** (3 μM in tris buffer) in a 3.5 mL quartz cuvette was irradiated with a 365 nm UV lamp (5 mW) with stirring. The emission spectra of the solution were recorded at different time points (0, 1, 3, 5, 7, 10, 15, 20, 30, 45, 60, 75 and 90 min). The data were processed with OriginLab Origin 6.0. The plot of I/I_0 @ 426 nm vs. time (Figure 2.) fits the equation:

$$y = y_0 + A e^{-kt}$$

to obtain the pseudo-first order rate constant k (39). Where I_0 and I are the initial emission intensity and the emission intensity after period of time t of UV light irradiation respectively.

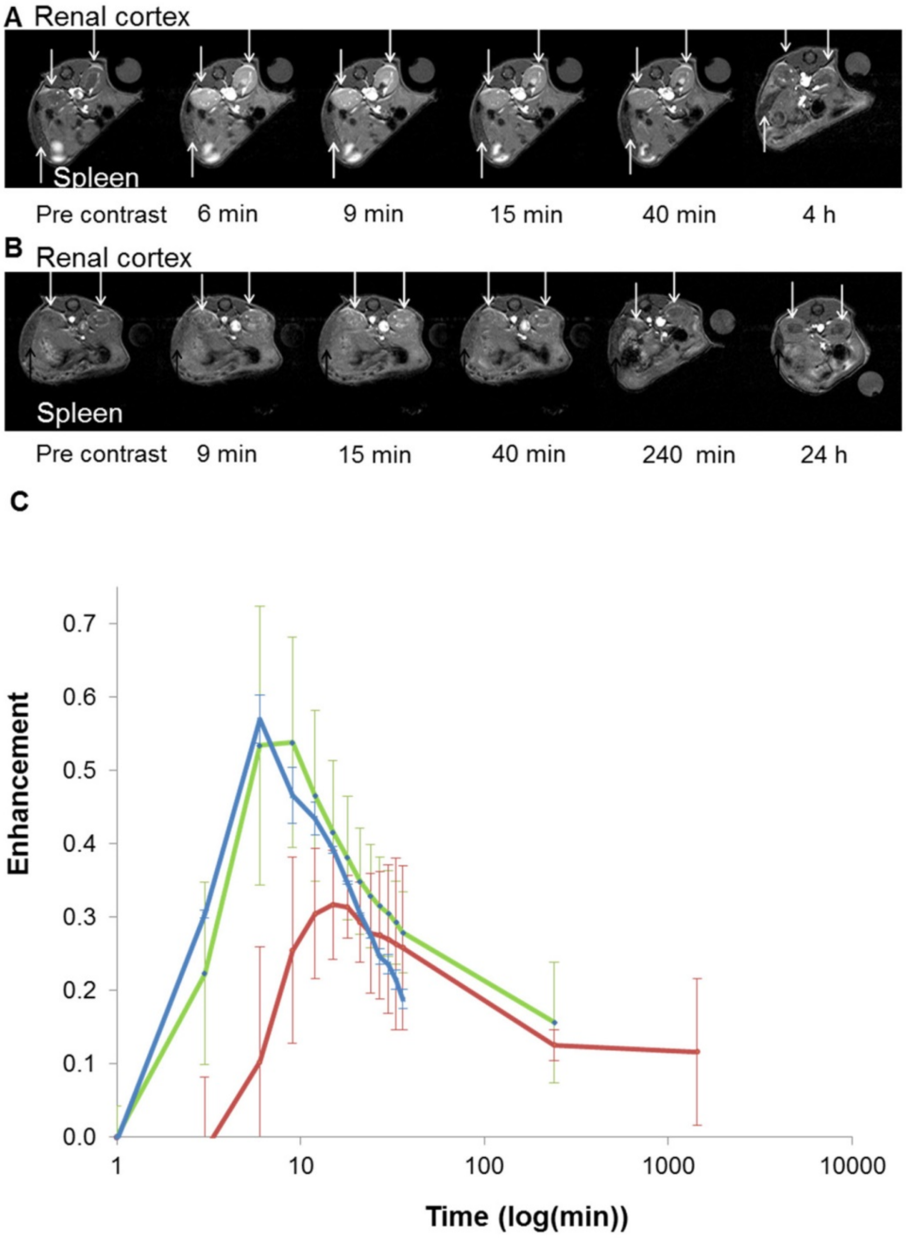

Figure 6. *In vivo* T_1-weighted MR images of mouse renal cortex between 6 minutes and 4 hours for **GdL** (A) and between 9 minutes and 24 hours for **PtGdL** (B). Signal-decay curves (red line: **PtGdL**, green line: **GdL**, blue line: Gd-DOTA) are represented in (C).

T1 relaxivity measurements

The $1/T_1$ nuclear magnetic relaxation dispersion (NMRD) profiles of Gd-DOTA, **GdL** and **PtGdL** (1mM) were recorded at 37 ^{o}C and 25 ^{o}C on a Stelar SMARtracer FFC fast-field-cycling relaxometer covering magnetic fields from 2.35 x 10^{-4} T to 0.25 T, which corresponds to a proton Larmor frequency range of 0.01-10 MHz. The temperature was controlled by a VTC91 temperature control unit and maintained by a gas flow. The temperature was determined according to previous calibration with a Pt resistance temperature probe. The accurate concentration of the solutions was determined by Inductively Coupled Plasma Mass Spectrometry (ICP-MS).

A set of 5 solutions with concentrations 5.4 µM to 0.1 mM were prepared and their Gd(III) concentration confirmed by ICP-MS, measured in a PerkinElmer NexION 350D spectrometer. The T_1 values of these solutions were measured in a 3 T Philips Achieva scanner (25 °C), using a MOLLI sequence. The T_1 value used for the determination of the relaxivity is the average of 3 slices for each sample.

Cell culture

Human cervical cancer HeLa cells were grown in Dulbecco's Modified Eagle Medium (DMEM). Human prostate stromal - WPMY-1 cells were obtained from the cell resource center of Shanghai Institute of Biological Sciences, Chinese Academy of Sciences. WPMY-1 is growth in MEM (GIBCO 41500034) and supplemented with 10% (v/v) fetal bovine serum, 1% penicillin and streptomycin at 37 ^{o}C and 5 % CO_2.

MTT cell cytotoxicity assays

For the dark cytotoxicity, HeLa or WPMY-1 cells were treated with testing complexes for 24 hours at 6 concentrations (0, 1, 5, 10, 20 and 40 µM). The cell monolayers were rinsed with phosphate buffer saline (PBS) once and incubated with 0.5 mg/mL MTT (3-(4, 5-dimethylthiazol-2-yl)-2 and 5-diphenyltetrazolium bromide) solution. The cellular inhibitory potency of the complexes was examined by the formation of formazan after addition of MTT for 3 hours to allow formazan production during cell metabolism. After that, formazan was fully dissolved in DMSO through oscillation. Finally, the absorbance of solution was measured with Biotek Power wave xsMicroplate Reader at the wavelength of 570 nm and 690 nm.

For the Photo-cytotoxicity, HeLa or WPMY-1 cells (3 x 10^3) were treated with testing complexes for 24 hours at 6 concentrations (0, 1, 5, 10, 20 and 40 µM). Afterward, the cells were exposed to UVA light (365 nm, 1 J/cm^2). Cell viability was determined by the MTT reduction assay at 24-hour post light irradiation.

Two-photon induced activation and fluorescence *in vitro* imaging

The cells were incubated with **PtGdL** (1, 2, 5, 10 µM) for 12 hours. The complexes (cell impermeable and dissolved in the medium) were washed out with PBS buffer. The cells with complexes were placed in a tissue culture chamber (5% CO_2, 37 ^{o}C) inside the two-photon confocal microscope. *In vitro* images were captured by using the Leica SP8 (upright configuration) confocal microscope which was equipped with a femto-second laser (wavelength: 700 to 1000 nm) and 40x/60x oil immersion objective. The *in vitro* images were taken after 30 min laser excitation (λ_{ex} = 700 nm, Power = 420 mW, each 5 min with 1 min laser excitation, steady temperature = 37^{o}C ± 1.5^{o}C).

Photo-induced *in vivo* tumor inhibition of PtGdL

Hela xenografts tumor nodules were implanted subcutaneously in the BALB/c nude mice (1 × 10^7 HeLa cells in 100 µL). Tumor nodules were allowed to grow to the volume about 100 mm^3 before initiating the treatment. Three mice with tumors in nearly the same volume were picked up and used for the treatment. Tumor length and width were measured with calipers, and the tumor volume was calculated as (length × width)^2/2.

T_1 weighted *in vivo* imaging and bio-distribution

Biodistribution studies were conducted on a 7T micro MRI system (Bruker, Wissembourg, France) equipped with a ^{1}H radiofrequency linear coil birdcage probe of 4 cm inner diameter in order to assess the uptake and clearance of MRI contrast agents (CA) from kidney, muscle, spleen, liver. All animal experiments were performed in accordance with the institutional animal protocol guidelines in place at Paris Descartes University, (saisine CEEA34.JS.142.1) and approved by the Institute's Animal Research Committee.

Wild-type female 8 weeks BALB/c mice (Elevage Janvier, Le Genest-St-Isle, France) were anaesthetized with isoflurane (1.5%, with air/O_2 0.5/0.25 L.min^{-1}) inhalation and placed in a dedicated contention cradle. 300 µL of gadolinium complexes in 0.9% physiological serum were intravenously injected via the tail vein while the mouse was in the scanner.

The scanning protocol was developed using Bruker Paravision 5.1 software. DCE Dynamic contrast enhanced sequence was recorded using Intragate Flash multislices for motion free artifacts T_1 weighted sequence (TR = 100 ms, TE = 4 ms, alpha = 80°). The final images have a spatial resolution of 236 μm x 236 μm in plane. The total scan time was in the order of 3 min 14 s per images. The dynamic follow-up was measured during in a scan time of 24 hours.

To study the biodistribution of each complex, several regions of interest (ROI) were monitored: the liver, muscle, spleen, kidney, and vessels. The corresponding MRI intensity related to the amount of the Gd complex contrast agents and was plotted versus time to visualize the uptake and clearance of each complex into the organs. Comparison with commercial Gd-DOTA (DOTAREM, Guerbet, France) was also performed at the corresponding concentration of Gd (10 mM).

Supplementary Material

Supplementary figures and tables.
http://www.ntno.org/v01p0186s1.pdf

Acknowledgment

This work is funded by the Hong Kong Baptist University (FRG2/15-16/009), PNCORE (F-HKBU203/14), Hong Kong Polytechnic University (HKPolyU), Hong Kong Research Grants Council (HKBU 12309516), Hong Kong Polytechnic University central Research Grant (G-UC08), HKBU-HKPolyU Joint Research Programme (RC-ICRS/15-16/02F-WKL02F-WKL) and a Royal Society International Exchange grant, Institut Weizmann Français Grant, CNRS, IDEX Programme interdisciplinaire, Université Paris Descartes and PHC PROCORE (project 33122PA).

Competing Interests

The authors have declared that no competing interest exists.

References

1. Smit E, Moro-Sibilot D, Carpeno Jde C, Lesniewski-Kmak K, Aerts J, Villatoro R, et al. Cisplatin and carboplatin-based chemotherapy in the first-line treatment of non-small cell lung cancer: Analysis from the European FRAME study. Lung Cancer. 2016; 92: 35-40.
2. Jungwirth U, Xanthos DN, Gojo J, Bytzek AK, Korner W, Heffeter P, et al. Anticancer activity of methyl-substituted oxaliplatin analogs. Mol Pharmacol. 2012; 81: 719-28.
3. Wang D, Lippard SJ. Cellular processing of platinum anticancer drugs. Nat Rev Drug Discov. 2005; 4: 307-20.
4. Dasari S, Tchounwou PB. Cisplatin in cancer therapy: molecular mechanisms of action. Eur J Pharmacol. 2014; 740: 364-78.
5. Abu-Surrah AS, Kettunen M. Platinum group antitumor chemistry: design and development of new anticancer drugs complementary to cisplatin. Curr Med Chem. 2006; 13: 1337-57.
6. Townsend DM, Shen H, Staros AL, Gate L, Tew KD. Efficacy of a glutathione S-transferase pi-activated prodrug in platinum-resistant ovarian cancer cells. Mol Cancer Ther. 2002; 1: 1089-95.
7. Yoong SL, Wong BS, Zhou QL, Chin CF, Li J, Venkatesan T, et al. Enhanced cytotoxicity to cancer cells by mitochondria-targeting MWCNTs containing platinum(IV) prodrug of cisplatin. Biomaterials. 2014; 35: 748-59.
8. Pathak RK, Marrache S, Choi JH, Berding TB, Dhar S. The prodrug platin-A: simultaneous release of cisplatin and aspirin. Angew Chem Int Ed Engl. 2014; 53: 1963-7.
9. Kumar R, Shin WS, Sunwoo K, Kim WY, Koo S, Bhuniya S, et al. Small conjugate-based theranostic agents: an encouraging approach for cancer therapy. Chem Soc Rev. 2015; 44: 6670-83.
10. Avaji PG, Park JH, Lee HJ, Jun YJ, Park KS, Lee KE, et al. Design of a novel theranostic nanomedicine: synthesis and physicochemical properties of a biocompatible polyphosphazene-platinum(II) conjugate. Int J Nanomedicine. 2016; 11: 837-51.
11. Pan D. Theranostic nanomedicine with functional nanoarchitecture. Mol Pharm. 2013; 10: 781-2.
12. Rizzo LY, Theek B, Storm G, Kiessling F, Lammers T. Recent progress in nanomedicine: therapeutic, diagnostic and theranostic applications. Curr Opin Biotechnol. 2013; 24: 1159-66.
13. Prabhu P, Patravale V. The upcoming field of theranostic nanomedicine: an overview. J Biomed Nanotechno. 2012; 8: 859-82.
14. Dai Y, Xiao H, Liu J, Yuan Q, Ma P, Yang D, et al. In vivo multimodality imaging and cancer therapy by near-infrared light-triggered trans-platinum pro-drug-conjugated upconverison nanoparticles. J Am Chem Soc. 2013; 135: 18920-9.
15. Li Y, Lin TY, Luo Y, Liu Q, Xiao W, Guo W, et al. A smart and versatile theranostic nanomedicine platform based on nanoporphyrin. Nat Commun. 2014; 5: 4712.
16. Lammers T, Aime S, Hennink WE, Storm G, Kiessling F. Theranostic Nanomedicine. Acc Chem Res. 2011; 44: 1029-38.
17. Chen HP, Chen MH, Tung FI, Liu TY. A Novel Micelle-Forming Material Used for Preparing a Theranostic Vehicle Exhibiting Enhanced in Vivo Therapeutic Efficacy. J Med Chem. 2015; 58: 3704-19.
18. Min Y, Li J, Liu F, Yeow EK, Xing B. Near-infrared light-mediated photoactivation of a platinum antitumor prodrug and simultaneous cellular apoptosis imaging by upconversion-luminescent nanoparticles. Angew Chem Int Ed Engl. 2014; 53: 1012-6.
19. Yuan Y, Kwok RT, Tang BZ, Liu B. Targeted theranostic platinum(IV) prodrug with a built-in aggregation-induced emission light-up apoptosis sensor for noninvasive early evaluation of its therapeutic responses in situ. J Am Chem Soc. 2014; 136: 2546-54.
20. Zheng M, Wang Y, Shi H, Hu Y, Feng L, Luo Z, et al. Redox-mediated disassembly to build activatable trimodal probe for molecular imaging of biothiols. ACS Nano. 2016; 10: 10075-85.
21. Lv R, Yang P, He F, Gai S, Yang G, Dai Y, et al. An imaging-guided platform for synergistic photodynamic/photothermal/chemo-therapy with pH/temperature-responsive drug release. Biomaterials. 2015; 63: 115-27.
22. Hayashi K, Nakamura M, Miki H, Ozaki S, Abe M, Matsumoto T, et al. Magnetically responsive smart nanoparticles for cancer treatment with a combination of magnetic hyperthermia and remote-control drug release. Theranostics. 2014; 4: 834-44.
23. Li H, Lan R, Chan CF, Jiang L, Dai L, Kwong DW, et al. Real-time in situ monitoring via europium emission of the photo-release of antitumor cisplatin from a Eu-Pt complex. Chem Commun (Camb). 2015; 51: 14022-5.
24. Huang CC, Su CH, Li WM, Liu TY, Chen JH, Yeh CS. Bifunctional Gd2O3/C Nanoshells for MR Imaging and NIR Therapeutic Applications. Adv Funct Mater. 2009; 19: 249-58.
25. Huang P, Rong P, Jin A, Yan X, Zhang MG, Lin J, et al. Dye-loaded ferritin nanocages for multimodal imaging and photothermal therapy. Adv Mater. 2014; 26: 6401-8.
26. Yue C, Liu P, Zheng M, Zhao P, Wang Y, Ma Y, et al. IR-780 dye loaded tumor targeting theranostic nanoparticles for NIR imaging and photothermal therapy. Biomaterials. 2013; 34: 6853-61.
27. Ye D, Shuhendler AJ, Pandit P, Brewer KD, Tee SS, Cui L, et al. Caspase-responsive smart gadolinium-based contrast agent for magnetic resonance imaging of drug-induced apoptosis. Chem Sci. 2014; 4: 3845-52.
28. Deng Y, Bartholomeyzik T, Backvall JE. Control of selectivity in palladium-catalyzed oxidative carbocyclization/borylation of allenynes. Angew Chem Int Ed Engl. 2013; 52: 6283-7.
29. Cao CY, Shen YY, Wang JD, Li L, Liang GL. Controlled intracellular self-assembly of gadolinium nanoparticles as smart molecular MR contrast agents. Sci Rep. 2013; 3: 1024.
30. Du W, Yuan Y, Wang L, Cui YS, Wang H, Xu HQ, et al. Multifunctional bioconjugate for cancer cell-targeted theranostics. Bioconjug Chem. 2015; 26: 2571-8.
31. Aime S, Batsanov AS, Botta M, Howard JAK, Lowe MP, Parker D. Structure and relaxivity of macrocyclic gadolinium complexes incorporating pyridyl and 4-morpholinopyridyl substituents. New J Chem 1999; 23: 669-70.
32. Zhu ZZ, Wang XY, Li TJ, Aime S, Sadler PJ, Guo ZJ. Platinum(II)-gadolinium(III) complexes as potential single-molecular theranostic agents for cancer treatment. Angew Chem Int Ed Engl. 2014; 53: 13225-8.

33. Messori L, Merlino A. Cisplatin binding to proteins: molecular structure of the Ribonuclease A adduct. Inorg Chem. 2014; 53: 3929-31.
34. Casini A, Gabbiani C, Mastrobuoni G, Messori L, Moneti G, Pieraccini G. Exploring metallodrug-protein interactions by ESI mass spectrometry: The reaction of anticancer platinum drugs with horse heart cytochrome c. ChemMedChem. 2006; 1: 413-7.
35. Xue S, Qiao J, Jiang J, Hubbard K, White N, Wei L, et al. Design of ProCAs (protein-based Gd(3+) MRI contrast agents) with high dose efficiency and capability for molecular imaging of cancer biomarkers. Med Res Rev. 2014; 34: 1070-99.
36. Timerbaev AR, Hartinger CG, Aleksenko SS, Keppler BK. Interactions of antitumor metallodrugs with serum proteins: Advances in characterization using modern analytical methodology. Chem Rev. 2006; 106: 2224-48.
37. Krauss IR, Ferraro G, Merlino A. Cisplatin-protein Interactions: unexpected drug binding to N-Terminal amine and lysine side chains. Inorg Chem. 2016; 55: 7814-6.
38. Bunzli JCG. Lanthanide luminescence for biomedical analyses and imaging. Chem Rev. 2010; 110: 2729-55.
39. Sassin NA, Everhart SC, Dangi BB, Ervin KM, Cline JI. Fluorescence and photodissociation of rhodamine 575 cations in a quadrupole ion trap. J Am Soc Mass Spectrom. 2009; 20: 96-104.